The Seismic Record
A journal of the Seismological Society of America

Preliminary Observations of the 5 April 2024 M_w 4.8 New Jersey Earthquake

Oliver S. Boyd[*1], William D. Barnhart[1], James Bourke[2], Martin Chapman[3], Paul S. Earle[1], Guo-chin Dino Huang[4], Jessica A. Thompson Jobe[1], Won-Young Kim[5], Frederik Link[6], Mairi Litherland[7], Andrew Lloyd[5], Maureen D. Long[6], Sara McBride[1], Andrew J. Michael[8], Walter D. Mooney[8], Gregory S. Mountain[2], Sissy Nikolaou[9], Alexandros Savvaidis[4], Felix Waldhauser[5], Cecily J. Wolfe[10], and Clara Yoon[11]

Abstract

On 5 April 2024, 10:23 a.m. local time, a moment magnitude 4.8 earthquake struck Tewksbury Township, New Jersey, about 65 km west of New York City. Millions of people from Virginia to Maine and beyond felt the ground shaking, resulting in the largest number (>180,000) of U.S. Geological Survey (USGS) "Did You Feel It?" reports of any earthquake. A team deployed by the Geotechnical Extreme Events Reconnaissance Association and the National Institute of Standards and Technology documented structural and nonstructural damage, including substantial damage to a historic masonry building in Lebanon, New Jersey. The USGS National Earthquake Information Center reported a focal depth of about 5 km, consistent with a lack of signal in Interferometric Synthetic Aperture Radar data. The focal mechanism solution is strike slip with a substantial thrust component. Neither mechanism's nodal plane is parallel to the primary northeast trend of geologic discontinuities and mapped faults in the region, including the Ramapo fault. However, many of the relocated aftershocks, for which locations were augmented by temporary seismic deployments, form a cluster that parallels the general northeast trend of the faults. The aftershocks lie near the Tewksbury fault, north of the Ramapo fault.

Cite this article as Boyd, O. S., W. D. Barnhart, J. Bourke, M. Chapman, P. S. Earle, G. Huang, J. A. Thompson Jobe, W.-Y. Kim, F. Link, M. Litherland, et al. (2024). Preliminary Observations of the 5 April 2024 M_w 4.8 New Jersey Earthquake, *The Seismic Record*. **4**(**4**), 240–250, doi: 10.1785/0320240024.

Supplemental Material

Introduction

Earthquakes in plate interiors are relatively rare and difficult to forecast. In the central and eastern United States (CEUS), a stable continental region of North America, tectonic earthquakes (i.e., not triggered by human activity) with magnitude (M) greater than 3, not including foreshocks, aftershocks, or induced events (Petersen *et al.*, 2023), occur about 20 times per year (Sykes *et al.*, 2008). In contrast, earthquakes greater than M 3 in California, which hosts the right-lateral strike-slip boundary between the North American and Pacific plates, generally occur at least 10 times more often (based on analysis of wmm_104.c2 seismicity catalog in Petersen *et al.*, 2023). Moreover, earthquakes near plate boundaries can often be associated with mapped faults having documented Quaternary offset, whereas few active faults are recognized in the CEUS (Jobe *et al.*, 2022). Regardless, several moderate- to large-magnitude earthquakes have occurred along the eastern United States in the last few hundred years, including the 1755 (estimated) M 6 Cape

1. U.S. Geological Survey, Golden, Colorado, U.S.A., https://orcid.org/0000-0001-9457-0407 (OSB); https://orcid.org/0000-0003-0498-1697 (WDB); https://orcid.org/0000-0002-3500-017X (PSE); https://orcid.org/0000-0001-5574-4523 (JATJ); 2. Department of Earth and Planetary Sciences, Rutgers University, Piscataway, New Jersey, https://orcid.org/0000-0003-1399-5628 (JB); https://orcid.org/0000-0001-5221-0278 (GSM); 3. Department of Geosciences, Virginia Tech, Blacksburg, Virginia, U.S.A., https://orcid.org/0000-0003-2956-8305 (MC); 4. Bureau of Economic Geology, The University of Texas at Austin, Austin, Texas, U.S.A., https://orcid.org/0000-0002-2563-737X (GDH); https://orcid.org/0000-0001-6373-5256 (AS); 5. Lamont-Doherty Earth Observatory, Columbia University, Palisades, New York, U.S.A., https://orcid.org/0000-0002-0005-9681 (W-YK); https://orcid.org/0000-0002-1286-9737 (FW); 6. Department of Earth and Planetary Sciences, Yale University, New Haven, Connecticut, U.S.A., https://orcid.org/0000-0003-1639-0093 (FL); https://orcid.org/0000-0003-1936-3840 (MDL); 7. U.S. Geological Survey, Albuquerque Seismological Laboratory, Kirtland AFB, New Mexico, U.S.A., https://orcid.org/0009-0007-5175-5170 (ML); 8. U.S. Geological Survey, Moffett Field, California, U.S.A., https://orcid.org/0000-0002-2403-5019 (AJM); https://orcid.org/0000-0002-5310-3631 (WDM); 9. National Institute of Standards and Technology, Gaithersburg, Maryland, U.S.A., https://orcid.org/0000-0002-4094-2962 (SN); 10. U.S. Geological Survey, Reston, Virginia, U.S.A., https://orcid.org/0000-0003-3144-5697 (CJW); 11. U.S. Geological Survey, Pasadena, California, U.S.A., https://orcid.org/0000-0003-4521-3889 (CY)

*Corresponding author: olboyd@usgs.gov

Ann, Massachusetts (e.g., Monecke *et al.*, 2018), 1886 M 7 Charleston, South Carolina (e.g., Dutton, 1889; Pratt *et al.*, 2022), and the 2011 moment magnitude (M_w) 5.8 Mineral, Virginia (e.g., Horton *et al.*, 2015) earthquakes (Fig. 1 inset). These earthquakes did not occur on previously recognized faults, and they all caused damage. A global study of continental intraplate earthquakes found that moderate-to-large earthquakes preferentially occurred along rifted continental margins and identified eastern North America, including New Jersey, as one of these regions (Schulte and Mooney, 2005; Nikolaou *et al.*, 2012). Hence, for intraplate regions, rifted continental margins likely have a higher seismic hazard in comparison to nonrifted continental interiors.

The relatively low rate of present-day seismicity and lack of evidence of recent large surface ruptures in the CEUS contribute to the public's surprise when moderate events are felt. Such was the case when on 5 April 2024, at 10:23 a.m. local time, an earthquake of M_w 4.8 strongly shook Tewksbury Township, New Jersey. Like many moderate earthquakes in the CEUS, this event was felt widely due to the relatively competent crust in the region, compared to frequent fracturing and less competent crust near plate boundaries (Atkinson and Wald, 2007). The earthquake was felt by an estimated 42 million people from Virginia to Maine and beyond (Fig. 2) and garnered the largest number of felt reports for a single earthquake ever received by the U.S. Geological Survey (USGS).

Social implications and impacts

The mainshock had 183,755 felt reports (Fig. 2; see Data and Resources) with 10% of felt reports coming from New York City, ~65 km east of the epicenter, and Philadelphia, ~90 km to the south. The most felt reports came from within New York City and its immediate surroundings, which accounts for four of the eight highest reporting zip codes (n = 2546). Respondents from these top four zip codes in New York reported Modified Mercalli Intensities (MMIs) ranging from III to VI.

In addition, more than 2500 respondents filled out the long-form felt report, which now includes demographic and earthquake early warning questions; the added questions are outlined in Goltz *et al.* (2024). Respondents may have filled in these extra questions in response to two issues: (1) people self-reporting regarding received alerts from New York and New Jersey emergency management agencies not related to earthquake early warning; or (2) people who self-reported because they thought they should have received an alert but did not. The second option could have occurred because of confusion about where ShakeAlert, the earthquake early warning system for the West Coast of the United States, operates. Currently, ShakeAlert is only publicly available in Washington, Oregon, and California (McBride *et al.*, 2022).

The earthquake was three days after a large, damaging earthquake in Taiwan (M_w 7.4) and three days before a full solar eclipse, giving rise to alternative explanations that these events were connected (Miller, 2024). However, no other large or damaging earthquakes occurred on the day of the eclipse.

Earthquake intensities and ground motions

Shaking intensities exceeded an average of V on the MMI scale (moderate shaking—very light damage) within 10 km of the earthquake. The reconnaissance team deployed by the Geotechnical Extreme Events Reconnaissance (GEER) Association and the National Institute of Standards and Technology (NIST) documented the partial collapse of the stone façade of Taylor's Mill, a 264-year-old, pre-Revolutionary War unreinforced masonry structure 4 km south of the earthquake epicenter, east-northeast of the town of Lebanon, New Jersey (Fig. 3). The team also obtained first-hand accounts and archived media coverage of nonstructural damages such as objects falling from shelves and cracks in drywall. Observed ground motions at 70 km (the closest seismic station) and greater distance were consistent with the median Next Generation Attenuation ground-motion model for the CEUS (NGA-East; Goulet *et al.*, 2021), which was used in the most recent update of the USGS National Seismic Hazard Model (Petersen *et al.*, 2024). The largest measured peak ground acceleration was 20 cm/s^2 at 110 km epicentral distance, which is just over one standard deviation above the NGA-East prediction.

Geologic background

Numerous faults were previously mapped in the region of the Tewksbury earthquake, but none have been recognized as Quaternary active (i.e., class C faults; Crone and Wheeler, 2000). These faults follow the general trend of the Appalachian Mountains, striking north to northeast (Fig. 1) and dipping 45° or more to the southeast (Herman *et al.*, 1996). Many of the faults were formed during the closing of the Iapetus Ocean during Paleozoic mountain-building events (230–500 Ma) that created the Appalachian Mountains. They were reactivated as normal faults during Mesozoic rifting that formed the present-day Atlantic Ocean (Herman, 1992). These faults create a boundary between the New Jersey Highlands to the northwest, composed of Mesoproterozoic to Ordovician igneous and

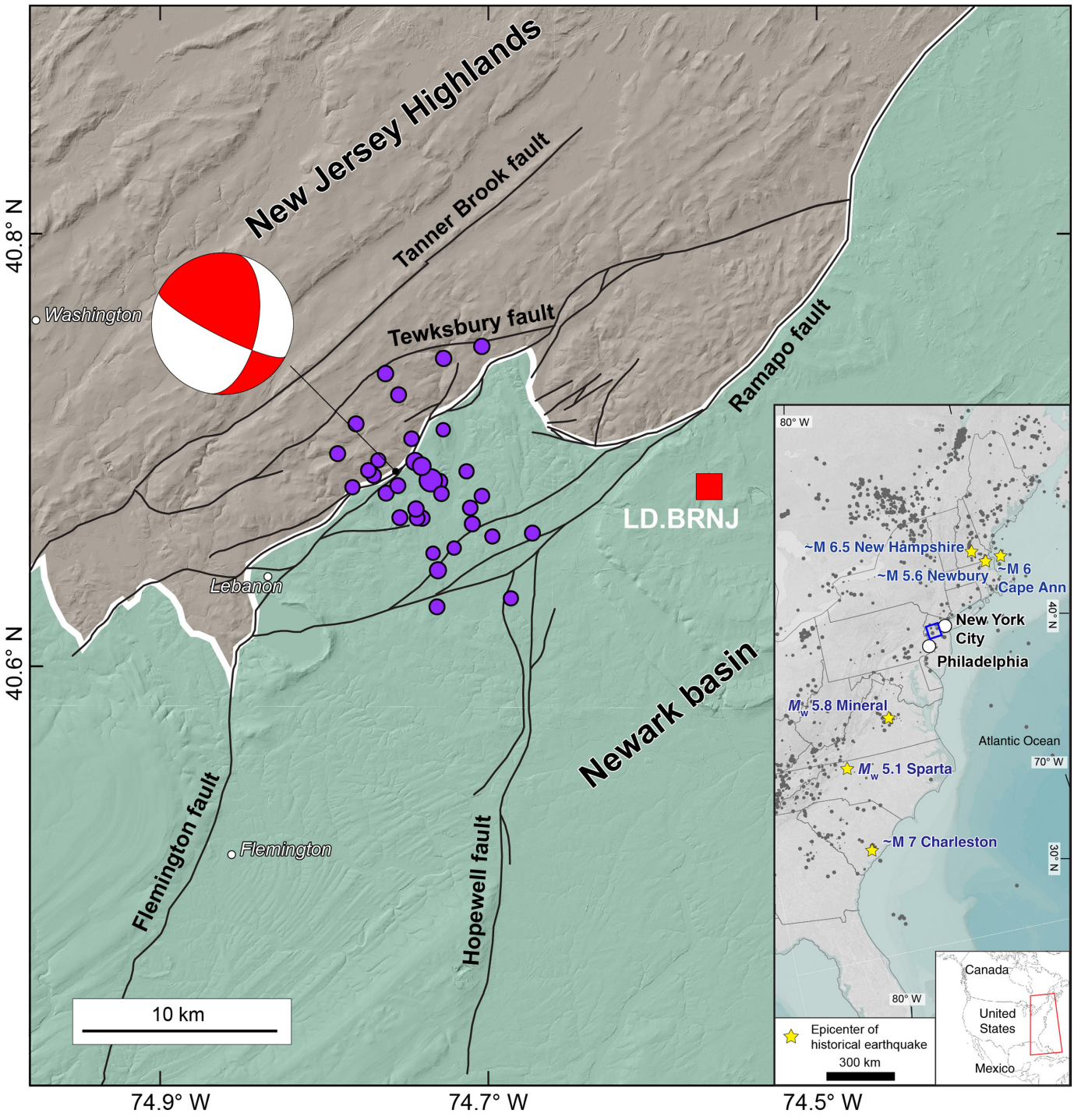

Figure 1. Geologic map of the epicentral area simplified from Owens *et al.* (1998) and Drake *et al.* (1996) draped over topography showing mapped faults (black lines), initial aftershock locations from U.S. Geological Survey (USGS) Comprehensive Earthquake Catalog (ComCat; U.S. Geological Survey [USGS], 2017; downloaded 7 April 2024, at 13:59 UTC; purple circles), and mainshock focal mechanism (see Data and Resources). The location of seismic station BRNJ, which was not recording during the mainshock, is shown by the red square. The New Jersey Highlands, composed of Mesoproterozoic to Ordovician igneous and metamorphic rocks, are shown to the northwest of the white line, and the Newark basin, composed of Mesozoic sedimentary and volcanic rocks, lies to the southeast. Background image is a shaded relief derived from the 10 m National Elevation Dataset (see Data and Resources). Seismicity in inset (gray dots and yellow stars) is from the USGS ComCat (USGS, 2017). The blue rectangle in the inset map indicates the region depicted in the larger figure.

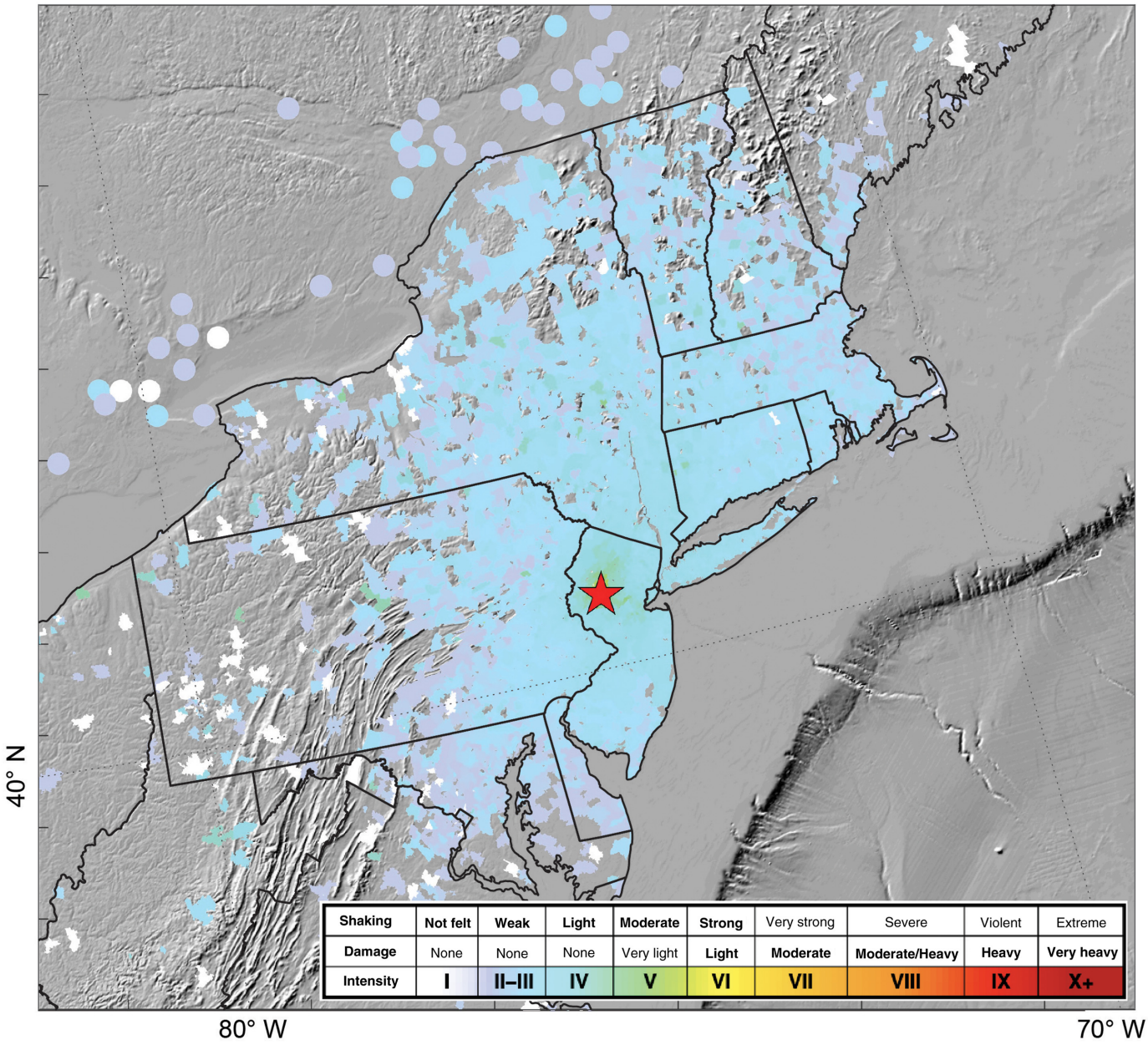

Figure 2. Distribution of "Did You Feel It?" responses in the northeastern United States and Canada aggregated by zip code and city geolocation. Intensity scale produced by the U.S. Geological Survey (see Data and Resources).

metamorphic rocks, and the Newark basin to the southeast, composed of rift-related Mesozoic sedimentary and volcanic rocks. The primary fault along this boundary is the northeast-striking Ramapo fault of the Ramapo fault system (Ratcliffe, 1971), which has raised concern, given that it traverses the New York metropolitan area. The fault system is composed of long continuous fault strands that have been reactivated with different kinematics in different stress regimes throughout its geologic history (Ratcliffe, 1971), although paleoseismic trenching of the fault did not reveal definitive evidence of Quaternary fault movement (Ratcliffe *et al.*, 1990). The northeast-trending fault strands that deform Mesoproterozoic, Paleozoic, and Mesozoic rocks typically have a brittle deformational fabric that consists of breccia, gouge, alteration, and retrogression of mafic mineral phases, fractures, or slickensides coated by chlorite or epidote, and close-spaced fracture cleavage (Volkert, 2021). Most of the initially determined earthquake locations (as of 7 April; U.S.

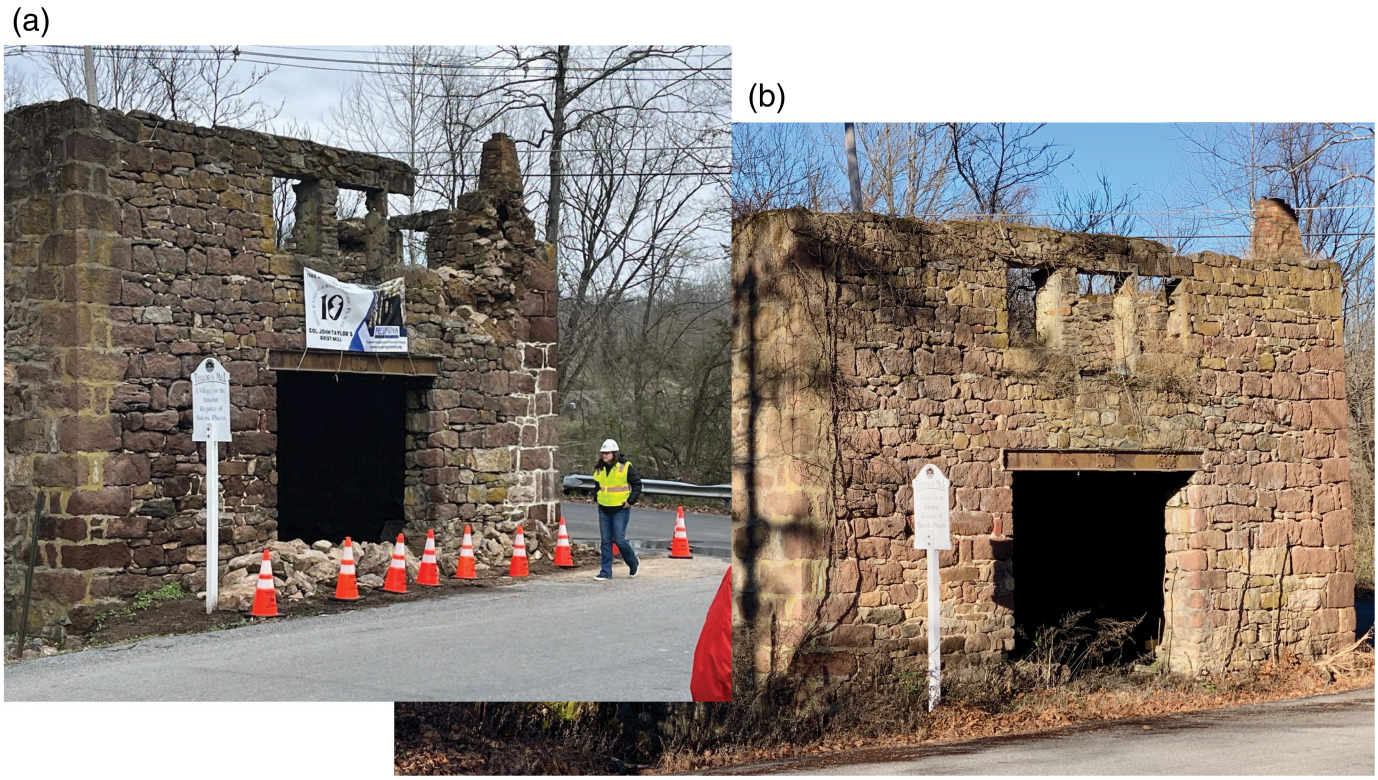

Figure 3. Photos of Taylor's Mill taken before and after the 5 April 2024, earthquake. (a) The photo was taken by the Geotechnical Extreme Events Reconnaissance Association and the National Institute of Standards and Technology (GEER–NIST) team. (b) The photo is obtained from the website in Data and Resources (photo by Zeete—Own work, CC BY-SA 4.0).

Geological Survey [USGS], 2017) do not lie along one of the northeast-trending strands of the Ramapo fault system (Fig. 1; Drake *et al.*, 1996). This is also the case for the focal plane orientations from the mainshock moment tensor solution for which the first nodal plane strikes 11° north-northeast and dips 45° southeast, and the second nodal plane strikes 117° east-southeast and dips 75° southwest.

Data Acquisition and Preliminary Analysis

Acquisition of Interferometric Synthetic Aperture Radar

After a large earthquake, usually greater than magnitude 5, data acquisition is critical, both to guide emergency response and to capture ephemeral information that may be erased by human activity and natural events. A Synthetic Aperture Radar image was acquired by the European Space Agency Sentinel-1 instrument ~8.5 hr after origin time on 5 April. We generated a coseismic interferogram (Fig. S1A, available in the supplemental material to this article) with a pre-event image acquired on 24 March. No appreciable surface deformation is observed, which is consistent with the estimates of hypocentral (derived from travel times) and moment tensor (derived from waveform modeling) depths of about 5 km (Mellors *et al.*, 2004; Shea and Barnhart, 2022). No surface deformation was found by the initial GEER–NIST reconnaissance team that scoured the epicentral region on foot. The absence of detectable surface deformation was confirmed with an independent interferogram that spanned 29 March to 10 April 2024 (Fig. S1B).

Seismic deployments

Permanent seismic stations that belong to the Lamont–Doherty Cooperative Seismic Network (LCSN) and the Pennsylvania State Seismic Network were closest (70–80 km) to the sequence and critical for monitoring the early aftershocks. LCSN stations close to the epicentral area were not operating at the time of the mainshock due to lack of funding support, but LD.BRNJ (Fig. 1), LD.ODNJ, and LD.PANJ stations were repaired and brought back online four days after the mainshock. In addition, multiple groups visited the area to deploy broadband and short-period seismometers to measure aftershocks. Lamont–Doherty Earth Observatory was the first to reach the area on 5 April, when it started deploying five short-period seismometers within 10 km

of the mainshock epicenter (Fig. 4). The first, RAMP1, had problems and is not shown. A sixth station, RAMP6, was installed on 30 April. The USGS began deploying on 9 April, followed by the University of Texas at Austin (TexNet) and Rutgers and Yale Universities. A total of 25 instruments were initially deployed (Table S1), and an additional 75 SmartSolo 4 Hz nodal seismometers were set out in three distinct subarrays within another two weeks. Seismometers were placed away from busy roads and fast-flowing streams on residential and business properties. The USGS and TexNet instruments are telemetered to the EarthScope Seismological Facility for the Advancement of Geoscience (SAGE) Data Management Center (DMC) in real time allowing for their use in locating aftershocks. As of 21 May 2024, 174 aftershocks with local magnitude (M_L) greater than 0.2 were reported by the USGS. The USGS aftershock forecast parameters from 17 May imply that about 70 M_L or greater aftershocks are expected from 17 May to 17 June. This forecast indicates that there will be numerous local earthquakes with which to analyze data from the temporary deployments.

Most stations of the rapid response deployment are scheduled to be in place for a period of several months; the SmartSolo nodal deployment, in particular, is limited by the ~1 month battery life of the nodes. However, six broadband stations deployed by TexNet and five broadbands deployed by Rutgers/Yale are scheduled to remain in the field for up to 6 months total to record aftershocks, ambient noise, and teleseisms that will be useful for studies of crustal velocities and structure. The five USGS and five temporary LCSN stations will remain in the field for at least 5 months or longer to record useful data. All data from the deployment are, or will be, publicly available as soon as data are archived. Data can be obtained via the EarthScope DMC using the following network codes: Lamont–Doherty Cooperative Seismographic Network stations (LD), USGS stations (GS), and TexNet and Rutgers/Yale broadband stations (4N). A network code for the Rutgers/Yale nodal deployment will be assigned when the data are archived.

Earthquake relocations and causative faults

Before the temporary aftershock deployments, the smallest magnitude aftershock in the area reported by the National Earthquake Information Center (NEIC) based on the available regional stations was about 1.3 (M_L). The temporary stations have reduced this to near 0, with horizontal location errors now averaging about 1.7 km. Vertical errors are now on the order of 3 km, but double-difference relocation (Waldhauser and Ellsworth, 2000) can reduce location uncertainties by a factor of 10 or more, especially with the use of many nearby temporary seismometers. Figure 5 shows a preliminary double-difference earthquake relocation analysis performed on manual arrival-time picks of aftershocks in the USGS Comprehensive Earthquake Catalog (ComCat; USGS, 2017) up to 4 June 2024, using the 1D velocity model of Wu *et al.* (2015). Refer to the supplemental tables for a list of additional permanent seismic stations used in the relocation analysis (Table S2), the original ComCat earthquake catalog (Table S3), and the relocated catalog (Table S4). Many of the relocated aftershocks lie along a northeast trend on a plane that dips about 50° southeast, which is generally consistent with the strike and dip of previously mapped bedrock faults near the epicentral region. However, the locations and depths of the aftershocks indicate that they may be on an unmapped fault that lies between the Flemington, Tewksbury, or Tanner Brook faults and may not reach the surface, based on prior geologic mapping and down-dip fault projections of ~45° (Drake *et al.*, 1996). Given that these faults are interpreted to become gentler in dip and merge at depth, their exact subsurface geometries and relationships remain unknown (e.g., Drake *et al.*, 1996), attributing the earthquake to a particular fault based on the surface trace remains challenging. However, the mainshock and aftershock locations so far indicate the Ramapo fault was not active during this earthquake.

Notably, a preliminary analysis of 1 m light detection and ranging (lidar)-derived bare earth digital elevation models (USGS, 2022) neither revealed any definitive evidence of preexisting scarps or other active fault-related features near Rockaway Creek in the epicentral region nor have fault scarps been recognized in prior surficial mapping (Stanford, 2016). Lidar-derived topography in the epicentral area shows several north-northeast-trending scarps and topographic lineaments that cross ridges and fluvial terraces composed of weathered gneiss and gneiss-derived colluvium (Stanford, 2016), but these lineaments cannot be traced for more than 1 km across the landscape.

Aftershock Forecasts

The USGS operational aftershock forecasts (Michael *et al.*, 2019) were activated for this sequence due to the large population within the felt area, despite the mainshock magnitude being under the usual threshold of M ≥ 5. ComCat was used to retrieve aftershock data and store the forecasts, which are available via the mainshock event page (see Data and Resources). The forecasts use a nonstationary Poisson rate of earthquakes with magnitude ≥M, $\lambda(t,M)$, following a mainshock with magnitude M_m, given by

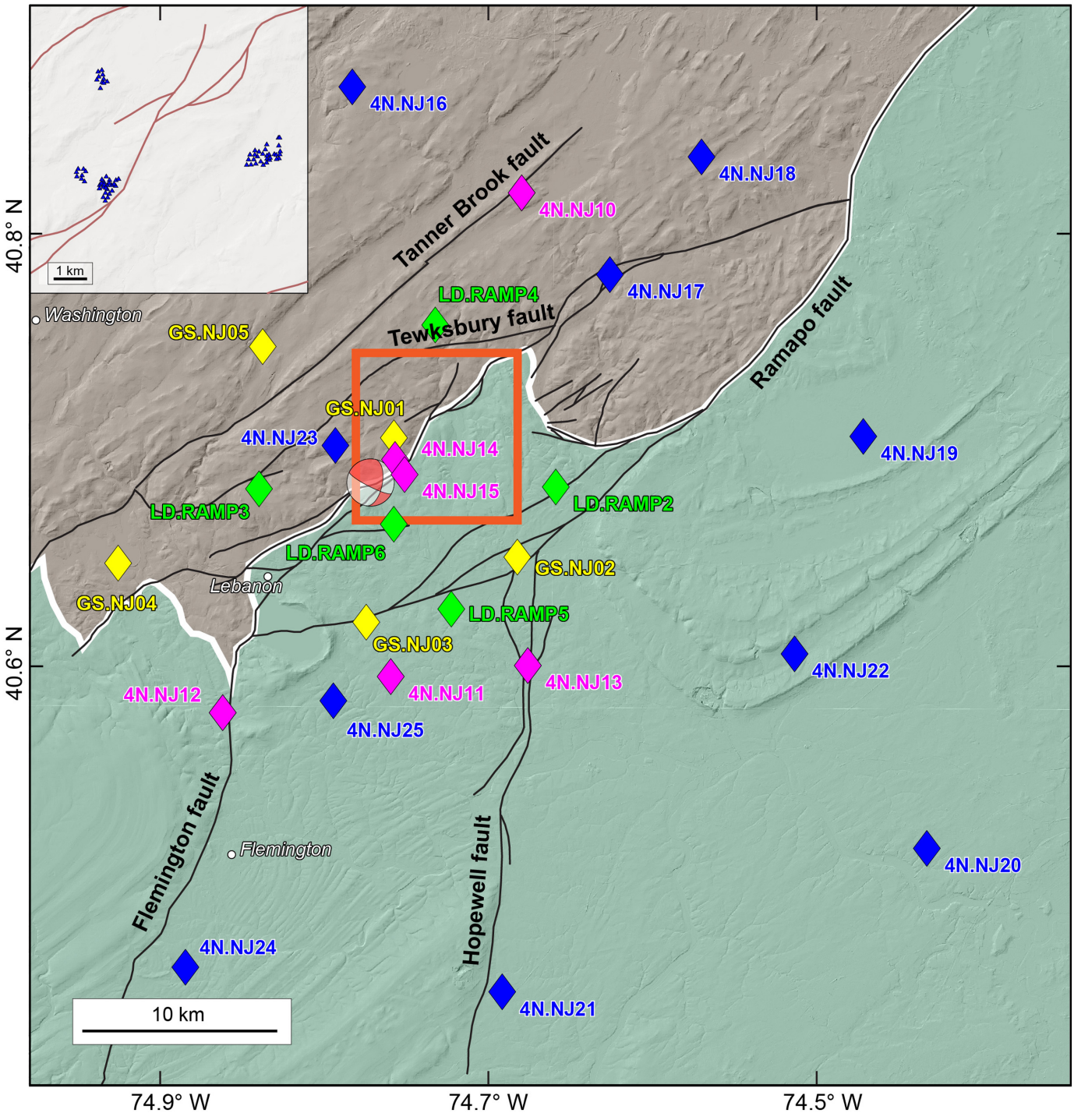

$$\lambda(t,M) = 10^{a+b(M_m-M)}(t+c)^{-p},$$

in which t is the time after the mainshock; a gives the productivity of the aftershock sequence; b is the slope of the Gutenberg–Richter distribution; and c and p are the parameters of the modified-Omori law (Reasenberg and Jones, 1989). The initial

Figure 4. Temporary seismometer deployments (diamonds): network code LD (green) indicates Lamont–Doherty Cooperative Seismographic Network; network code GS (yellow) indicates USGS; and network code 4N (magenta) indicates TexNet (blue) indicates Rutgers and Yale Universities. The blue triangles in the inset map (extent marked by orange box) are 75 nodal seismometers set out by Rutgers and Yale Universities.

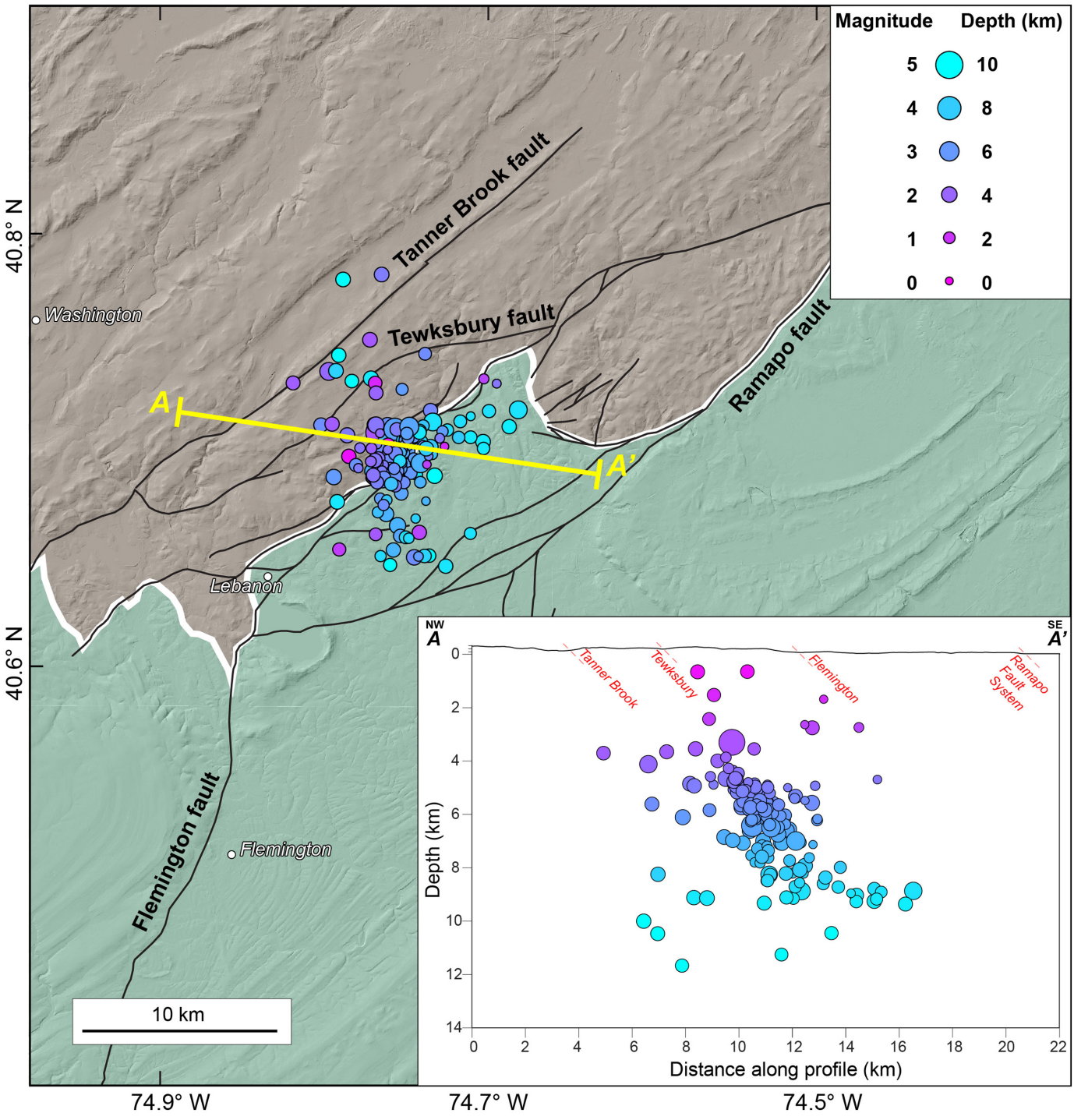

Figure 5. Double-difference earthquake relocations (circles) for aftershocks up to 4 June 2024, using differential travel times from the USGS ComCat (USGS, 2017) picks and singular value decomposition (Waldhauser and Ellsworth, 2000), and vertical profile along A–A′ from west-northwest to east-southeast, perpendicular to the N11E focal plane of the mainshock's focal mechanism available in ComCat (refer to Fig. 1). Topographic profile from 10 m National Elevation Dataset (see Data and Resources) and approximate fault locations and dips from Drake *et al.* (1996). Surficial fault dips projected to ~500 m depth; faults may become gentler and merge at depth.

forecast, starting 42 min after the mainshock, used generic parameters for stable continental regions (Page *et al.*, 2016). These parameters are $a = -2.85 \pm 0.867$ (1 standard deviation), $b = 1$, $c = 0.018$ days, and $p = 0.73$.

Four hours postmainshock, the automatic system began updating the a parameter based on observed aftershocks with M ≥ 3.5 and using the generic model as a Bayesian prior. To use aftershocks with M ≥ 2, forecasting was switched into a manual mode 8 hr postmainshock. The manual forecast process allowed adaptation to operations at the NEIC, which does not automatically and rapidly locate such small earthquakes, in this region. The aftershock parameters were estimated using only time periods when all M ≥ 2 aftershocks had been processed by the NEIC. The use of smaller aftershocks improved the resolution of the aftershock parameters, and the productivity increased to $a = -2.11 \pm 0.21$.

Two days postmainshock, it became clear that the sequence was decaying faster than implied by the generic model $p = 0.73$, and a change was made to determine a and p solely from the observed aftershocks. The initial sequence-specific forecast used $a = -2.5 \pm 0.23$ and $p = 1.05 \pm 0.24$. The data were insufficient to update the c and b parameters. The parameters were stable with declining uncertainties through the end of May when they were $a = -2.52 \pm 0.12$ and $p = 1.05 \pm 0.12$. At 13 days postmainshock, it was judged that the delay of up to 24 hr for the NEIC's daily analysis of small aftershocks had become inconsequential for the forecast calculations, and automatic forecasts were resumed. If the higher decay rate is common for this region, a localized model would improve forecasts in future, nearby sequences. However, the rare occurrence of aftershock sequences in this region could make that difficult.

Although the early forecasts overestimated the mean activity, the observations were within the 95% confidence bounds for all forecasts that finished within the first two months. The lower bound of the forecasts for M ≥ 3, 4, 5, 6, and 7 for the day and week following the forecast start time was 0. The only M ≥ 3 aftershock, so far, was an M 3.7 event 7.6 hr after the mainshock. That event was within the 95% confidence bounds for all the M ≥ 3 one-day and one-week forecasts issued before it occurred. The paucity of M ≥ 3 aftershocks and the presence of several M < 3 felt aftershocks during this aftershock sequence indicates the possible utility of issuing forecasts for smaller aftershocks in similar sequences.

Expectations for the Future

The causative fault that ruptured in the Tewksbury earthquake remains unknown. A large amount of seismic data is being acquired that could be used to locate aftershocks and active faults, constrain subsurface seismic velocity and basin structure, and improve estimates of seismic hazard in the region. Although the aftershock deployments are temporary, there is hope that this earthquake and what is being learned will motivate the community to better characterize active faults in the CEUS (their location and likely magnitude and return period), continue to expand the prehistoric record of earthquakes in this region, improve and maintain long-term seismic monitoring, and assess the risk due to relatively rare events in particularly vulnerable regions. This is especially true given the Tewksbury earthquake's proximity to the densely populated New York City metropolitan region with the majority of its building stock and infrastructure built before the first seismic code was applied in 1995 and for which safety and functional recovery of services are of major importance after any extreme event, including earthquakes.

Data and Resources

Felt reports and aftershock forecasts are available at the mainshock event page, https://earthquake.usgs.gov/earthquakes/eventpage/us7000ma74/executive. Scripts used to obtain ComCat events and pick and prepare the data for relocation are available at https://gitlab.com/cyoon1/NewJersey2024. Information regarding the Lamont–Doherty Cooperative Seismic Network (LD), temporary deployments by TexNet, Rutgers, and Yale (4N), Pennsylvania State Seismic Network (PE), and U.S. Geological Survey (USGS) (GS) seismic networks can be obtained from doi: 10.7914/SN/LD, doi: 10.7914/5ftj-a296, doi: 10.7914/SN/PE, and doi: 10.7914/SN/GS, respectively. In Figure 1, initial aftershock locations are obtained from the USGS Comprehensive Earthquake Catalog (ComCat; U.S. Geological Survey [USGS], 2017; downloaded 7 April 2024, at 13:59 UTC; purple circles), and mainshock focal mechanism (https://earthquake.usgs.gov/earthquakes/eventpage/us7000ma74/moment-tensor). The background image is a shaded relief derived from the 10 m National Elevation Dataset available at (https://apps.nationalmap.gov/downloader/). In Figure 2, the intensity scale produced by the USGS is obtained from https://usgs.github.io/shakemap/manual4_0/ug_intensity.html. Figure 3b is obtained from https://commons.wikimedia.org/w/index.php?curid=101194602. In Figure 5, the topographic profile from the 10 m National Elevation Dataset is available at https://apps.nationalmap.gov/downloader/. All websites were last accessed in September

2024. The supplemental material includes tables of the temporary seismic stations (Table S1), permanent seismic stations that were used to relocate the earthquakes (Table S2), and the original (Table S3), and relocated earthquake catalogs (Table S4). Also included is a figure showing Interferometric Synthetic Aperture Radar (InSAR) interferograms for the source region (Fig. S1).

Declaration of Competing Interests

The authors acknowledge that there are no conflicts of interest recorded.

Acknowledgments

The authors are grateful to Vadim Levin with the Center for Earthquake Research and Information at the University of Memphis for helping to facilitate communication and David Wald with the U.S. Geological Survey (USGS) for discussion regarding felt reports. The authors are appreciative of the USGS New Jersey Water Science Center for helping with the logistics for seismometer deployment. The authors are indebted to students, technicians, and researchers that helped with the deployment including Rasheed Ajala, Conor Bacon, Eric Beauce, Meritxell Colet, Evelyne Powell, Jake Tielke, Kaiwen Wang (all at Lamont–Doherty Earth Observatory), Steven Ploetz, Greg Tanner (both at USGS Albuquerque Seismological Laboratory), and Patrick Bowen (USGS New Jersey Water Science Center). The authors also are grateful to the residents near the epicenter who generously offered to host seismometers on their property. The authors also thank Thomas Pratt, Morgan Moschetti, Brian Shiro, Janet Carter, and two anonymous reviewers for thoughtful feedback that greatly improved the clarity and content of this article. Researchers at Lamont–Doherty Earth Observatory were supported by National Science Foundation (NSF) Division of Earth Sciences (EAR) Grant EAR-2431983, those at Yale University by NSF Grant EAR-2147536, and those at Rutgers by NSF grant EAR-2147426. The GEER team was supported by the NSF Division of Civil, Mechanical, and Manufacturing Innovation (CMMI) Award 1826118. Any use of trade, firm, or product names is for descriptive purposes only and does not imply endorsement by the U.S. Government. Certain trade names or company products are mentioned in the text to specify adequately the experimental procedure and equipment used. Neither does such identification imply recommendation or endorsement by the National Institute of Standards and Technology (NIST) nor does it imply that the equipment is the best available for the purpose. In this document, the authors have provided link(s) to website(s) that may have information of interest to our users. NIST does not necessarily endorse the views expressed or the facts presented on these sites. Furthermore, NIST does not endorse any commercial products that may be advertised or available on these sites.

References

Atkinson, G. M., and D. J. Wald (2007). "Did you feel it?" intensity data: A surprisingly good measure of earthquake ground motion, *Seismol. Res. Lett.* **78,** 362–368, doi: 10.1785/gssrl.78.3.362.

Crone, A. J., and R. L. Wheeler (2000). Data for Quaternary faults, liquefaction features, and possible tectonic features in the central and eastern United States, east of the Rocky Mountain front, *U.S. Geol. Surv. Open-File Rept. 2000-260*, 342 pp., doi: 10.3133/ofr00260.

Drake, A. A., R. A. Volkert, D. H. Monteverde, G. C. Herman, H. F. Houghton, R. A. Parker, and R. F. Dalton (1996). Bedrock geologic map of northern New Jersey, *U.S. Geol. Surv. Misc. Invest. Series Map I-2540-A*, scale 1:100,000, doi: 10.3133/i2540A.

Dutton, C. E. (1889). The Charleston earthquake of August 31, 1886, in *Ninth Annual Report of the U.S. Geological Survey to the Secretary of Interior*, J. W. Powell (Editor), United States Department of the Interior, U.S. Geological Survey, 203–528, doi: 10.3133/ar9.

Goltz, J. D., D. J. Wald, S. K. McBride, E. Reddy, V. Quitoriano, and J. K. Saunders (2024). The Ojai California earthquake of 20 August 2023: Earthquake early warning performance and alert recipient response in the M_w 5.1 event, *Seismol. Res. Lett.* doi: 10.1785/0220240023.

Goulet, C. A., Y. Bozorgnia, N. Kuehn, L. Al Atik, R. R. Youngs, R. W. Graves, and G. M. Atkinson (2021). NGA-East ground-motion characterization model part I: Summary of products and model development, *Earthq. Spectra* **37,** no. S1, 1231–1282, doi: 10.1177/87552930211018723.

Herman, G. C. (1992). Deep crustal structure and seismic expression of the central Appalachian orogenic belt, *Geology* **20,** 275–278.

Herman, G. C., D. H. Monteverde, R. A. Volkert, H. F. Houghton, R. A. Parker, A. A. Drake, and R. F. Dalton (1996). Cross sections of the Valley and Ridge, Highlands, and Piedmont Geologic Provinces, northern and central bedrock sheets, New Jersey, in *Bedrock Geologic Map of Northern New Jersey*, A. A. Drake, R. A. Volkert, D. H. Monteverde, G. C. Herman, H. F. Houghton, R. A. Parker, and R. F. Dalton (Editors), U.S. Geological Survey, U.S. Geol. Surv. Misc. Invest. Series Map I-2540-A, scale 1:100,000, doi: 10.3133/i2540A.

Horton, J. W., M. C. Chapman, and R. A. Green (2015). The 2011 Mineral, Virginia, earthquake, and its significance for seismic hazards in eastern North America—Overview and synthesis, in *The 2011 Mineral, Virginia, Earthquake, and its Significance for Seismic Hazards in Eastern North America*, M. Horton Jr., C. Chapman, and R. A. Green (Editors), Geological Society of America, Boulder, Colorado, Special Paper 509, 1–25, doi: 10.1130/2015.2509(01).

Jobe, J. T., A. Hatem, R. Gold, C. DuRoss, N. Reitman, R. Briggs, and C. Collett (2022). Revised earthquake geology inputs for the central and eastern United States and southeast Canada for the 2023 National Seismic Hazard Model, *Seismol. Res. Lett.* **93,** no. 6, 3100–3120, doi: 10.1785/0220220162.

McBride, S. K., H. Smith, M. Morgoch, D. Sumy, M. Jenkins, L. Peek, A. Bostrom, D. Baldwin, E. Reddy, R. D. Groot, *et al.* (2022). Evidence-based guidelines for protective actions and earthquake early warning systems, *Geophysics* **87,** no. 1, WA77–WA102, doi: 10.1190/geo2021-0222.1.

Mellors, R. J., H. Magistrale, P. Earle, and A. Cogbill (2004). Comparison of four moderate-size earthquakes in southern California using seismology and InSAR, *Bull. Seismol. Soc. Am.* **94,** no. 6, 2004–2014, doi: 10.1785/0120020219.

Michael, A. J., S. K. McBride, J. L. Hardebeck, M. Barall, E. Martinez, M. T. Page, N. V. D. Elst, E. H. Field, K. R. Milner, and A. M. Wein (2019). Statistical seismology and communication of the USGS operational aftershock forecasts for the 30 November 2018 M_w 7.1 Anchorage, Alaska, earthquake, *Seismol. Res. Lett.* **91,** 153–173, doi: 10.1785/0220190196.

Miller, K. (2024). Was today's earthquake connected to the solar eclipse? *New York Times*, available at https://www.nytimes.com/2024/04/05/science/total-solar-eclipse-earthquake.html (last accessed September 2024).

Monecke, K., F. G. McCarthy, J. B. Hubeny, J. E. Ebel, D. J. Brabander, S. Kielb, E. Howey, G. Janigian, and J. Pentesco (2018). The 1755 Cape Ann earthquake recorded in lake sediments of eastern New England: An interdisciplinary paleoseismic approach, *Seismol. Res. Lett.* **89,** no. 3, 1212–1222, doi: 10.1785/0220170220.

Nikolaou, S., J. E. Go, C. Z. Beyzaei, C. Moss, and P.W. Deming (2012). Geo-seismic design in the eastern United States: State of practice, *Paper Presented at GeoCongress 2012, Geotechnical Engineering State of the Art and Practice, American Society of Civil Engineering*, Oakland, California, 25–29 March 2012, doi: 10.1061/9780784412138.0030.

Owens, J. P., P. J. Sugarman, N. F. Sohl, R. A. Parker, H. F. Houghton, R. A. Volkert, A. A. Drake, and R. C. Orndorff (1998). Bedrock geologic map of central and southern New Jersey, *U.S. Geol. Surv. Misc. Invest. Series Map I-2540-B*, scale 1:100,000, doi: 10.3133/i2540B.

Page, M. T., N. V. D. Elst, J. Hardebeck, K. Felzer, and A. J. Michael (2016). Three ingredients for improved global aftershock forecasts: Tectonic region, time-dependent catalog incompleteness, and intersequence variability, *Bull. Seismol. Soc. Am.* **106,** 2290–2301, doi: 10.1785/0120160073.

Petersen, M. D., A. M. Shumway, P. M. Powers, E. H. Field, M. P. Moschetti, K. S. Jaiswal, K. R. Milner, S. Rezaeian, A. D. Frankel, A. L. Llenos, *et al.* (2023), Data release for the 2023 U.S. 50-state National Seismic Hazard Model, *U.S. Geol. Surv. Data Release*, doi: 10.5066/P9GNPCOD.

Petersen, M. D., A. M. Shumway, P. M. Powers, E. H. Field, M. P. Moschetti, K. S. Jaiswal, K. R. Milner, S. Rezaeian, A. D. Frankel, A. L. Llenos, *et al.* (2024). The 2023 U.S. 50-state National Seismic Hazard Model: Overview and implications, *Earthq. Spectra* **40,** no. 1, 5–88, doi: 10.1177/87552930231215428.

Pratt, T. L., A. K. Shah, R. Counts, J. J.W. Horton, and M. C. Chapman (2022). Shallow faulting in the epicentral area of the 1886 Charleston, South Carolina earthquake, *Bull. Seismol. Soc. Am.* **112,** no. 4, 2097–2123, doi: 10.1785/0120210329.

Ratcliffe, N. M. (1971). The Ramapo fault system in New York and adjacent northern New Jersey: A case of tectonic heredity, *Geol. Soc. Am. Bull.* **82,** 125–142.

Ratcliffe, N. M., W. C. Burton, and M. J. Pavich (1990). Orientation, movement history, and cataclastic rocks of Ramapo fault based on core drilling and trenching along the western margin of the Newark basin near Bernardsville, New Jersey, *U.S. Geol. Surv. Misc. Invest. Series Map I-1982*, scale 1:50,000, doi: 10.3133/i1982.

Reasenberg, P. A., and L. M. Jones (1989). Earthquake hazard after a mainshock in California, *Science* **243,** 1173–1176, doi: 10.1126/science.243.4895.1173.

Schulte, S. A., and W. D. Mooney (2005). An updated global earthquake catalog for stable continental regions: Reassessing the correlation with ancient rifts, *Geophys. J. Int.* **161,** no. 3, 707–721, doi: 10.1111/j.1365-246X.2005.02554.x.

Shea, H. N., and W. D. Barnhart (2022). The geodetic centroid (gCent) catalog: Global earthquake monitoring with satellite imaging geodesy, *Bull. Seismol. Soc. Am.* **112,** 2946–2957, doi: 10.1785/0120220072.

Stanford, S. D. (2016). Surficial geology of the Califon quadrangle, Hunterdon and Morris Counties, New Jersey, *New Jersey Geol. and Water Surv. Open-File Map series OFM 111*, scale 1:24,000, available at https://dep.nj.gov/wp-content/uploads/njgws/maps/ofmap/ofm111.pdf (last accessed September 2024).

Sykes, L. R., J. G. Armbruster, W.-Y. Kim, and L. Seeber (2008). Observations and tectonic setting of historic and instrumentally located earthquakes in the Greater New York City–Philadelphia area, *Bull. Seismol. Soc. Am.* **98,** 1696–1719, doi: 10.1785/0120070167.

U.S. Geological Survey (USGS) (2017). Advanced National Seismic System (ANSS) comprehensive catalog of earthquake events and products, *U.S. Geol. Surv. Earthquake Hazards Program*, doi: 10.5066/F7MS3QZH.

U.S. Geological Survey (USGS) (2022). USGS original product resolution NJ_NW_New_Jersey_6_County_Lidar_2017_B17, *U.S. Geol. Surv.*, available at https://apps.nationalmap.gov/downloader/ (last accessed September 2024).

Volkert, R. A. (2021). Bedrock geologic map of the Califon quadrangle, Hunterdon and Morris Counties, New Jersey, *New Jersey Geol. and Water Surv. Open-File Map OFM-133*, scale 1:24,000, available at https://dep.nj.gov/wp-content/uploads/njgws/maps/ofmap/ofm133.pdf (last accessed September 2024).

Waldhauser, F., and W. L. Ellsworth (2000). A double-difference earthquake location algorithm: Method and application to the northern Hayward fault, *Bull. Seismol. Soc. Am.* **90,** 1353–1368, doi: 10.1785/0120000006.

Wu, Q., M. C. Chapman, and J. N. Beale (2015). The aftershock sequence of the 2011 Mineral, Virginia, earthquake: Temporal and spatial distribution, focal mechanisms, regional stress, and the role of Coulomb stress transfer, *Bull. Seismol. Soc. Am.* **105,** no. 5, 2521–2537, doi: 10.1785/0120150032.

Manuscript received 4 July 2024
Published online 1 October 2024